Possibilities and limitations of the Prevost model for the modelling of cohesionless soil cyclic behaviour.

Possibilités et limitations du modèle de Prévost pour la modélisation du comportement cyclique des sols sans cohésion.

Cerfontaine B.[1,2], Charlier R.[1], Collin F.[1]
[1] *University of Liège, Department of Architecture, Geology and Constructions, Geotechnical Engineering Division, Chemin des chevreuils, 1, B52/3, 4000 Liège, Belgium*
[2] *FRIA, F.R.S.-FNRS, National Fund for Scientific Research, 1000, Bruxelles, Belgium*

ABSTRACT: The Prevost's model is currently used to model cyclic behaviour of soils especially in earthquake engineering. The original model is able to capture the main features of cyclic behaviour: pore pressure build up and plastic deformation accumulation. But accurate modelling of laboratory tests requires improvements. Enhanced models exist but require a lot of parameters that make them cumbersome for practical purpose. A suction caisson, part of a tripod offshore foundation for wind turbines is modelled. Possibilities of the Prevost's model are highlighted compared with a classical Drucker-prager model.

RÉSUMÉ : Le modèle de Prévost est couramment utilisé pour modéliser le comportement cyclique des sols, notamment dans l'ingénierie sismique. Le modèle original permet la représentation des caractéristiques principales de ce genre de comportement : une accumulation des pressions d'eau et déformations plastiques. Cependant, la représentation précise d'essais de laboratoire nécessite des modifications du modèle. Ces améliorations existent mais au prix d'un grand nombre de paramètres additionnels, ce qui rend malaisée son utilisation en pratique. Un caisson à succion, partie d'une fondation tripode d'éolienne offshore a été modélisé. Le sol est représenté alternativement par un modèle classique de Drucker-Prager puis par le modèle de Prevost afin de souligner les apports de celui-ci.

KEYWORDS: soil mechanics ; cyclic behaviour ; foundations ; constitutive behaviour

1 INTRODUCTION

Modelling the cyclic behaviour of soils is a crucial issue for earthquake engineering as well as for designing offshore wind turbines. This topic of interest is still an ongoing domain (Houlsby, et al., 2005). Despite its drawbacks, the Prevost's model, based on nested surfaces and non-associated plasticity is able to capture hysteretic behaviour of soils under cyclic loading.

1.1 *Definitions*

The sign convention of soil mechanics is applied, compressive stresses and strains are positive. The Macauley brackets $\langle\ \rangle$ are defined according to:

$$\langle \mathrm{f} \rangle = \begin{cases} 0, & x < 0 \\ \mathrm{f}, & x \geq 0 \end{cases} \tag{1}$$

':' indicates a dot product between two tensors (in bold characters) of the same order: for example $\boldsymbol{\sigma}:\boldsymbol{\sigma} = \sigma_{ij} \cdot \sigma_{ij}$ in index notation. If $\boldsymbol{\sigma}'$is the effective (Cauchy) stress tensor and $p' = 1/3 \cdot \boldsymbol{\sigma}':\boldsymbol{\delta}$ is the mean effective stress, then the deviatoric stress tensor ($\boldsymbol{s}$) is defined through

$$\mathbf{s} = \boldsymbol{\sigma}' - \mathrm{p}' \cdot \boldsymbol{\delta} \tag{2}$$

where $\boldsymbol{\delta}$ is the identity tensor.

1.2 *Constitutive equations*

The Prevost's model lies within the framework of elasto-plasticity. Constitutive equations are written in incremental form. The equation below links the effective stress rate $\dot{\boldsymbol{\sigma}}'$ to the elastic deformation rate $\dot{\boldsymbol{\epsilon}} - \dot{\boldsymbol{\epsilon}}^p$

$$\dot{\boldsymbol{\sigma}}' = \mathbf{E} : (\dot{\boldsymbol{\epsilon}} - \dot{\boldsymbol{\epsilon}}^{\mathrm{p}}) \tag{3}$$

where $\mathbf{E}$ is the isotropic fourth-order tensor of elastic coefficients. The plastic rate of deformation $\dot{\boldsymbol{\epsilon}}^{\mathrm{p}}$ is defined through

$$\dot{\boldsymbol{\epsilon}}^{\mathrm{p}} = \mathbf{P} \cdot \langle \mathrm{L} \rangle \tag{4}$$

where $\mathbf{P}$ is a symmetric second order tensor, defining a plastic potential. The plastic loading function is a scalar that depicts the amount of plastic deformation and is defined in the following

$$\mathrm{L} = \frac{1}{\mathrm{H}'} \cdot \mathbf{Q}:\dot{\boldsymbol{\sigma}}' \tag{5}$$

where $\mathbf{Q}$ is a second-order tensor defining the unit outer normal to the yield surface and H' the plastic modulus associated to this surface. This normal tensor can be decomposed into its deviatoric and dilationnal parts as

$$\mathbf{Q} = \mathbf{Q}' + \mathrm{Q}'' \cdot \boldsymbol{\delta} \tag{6}$$

1.3 *Yield functions*

The model is made of conical nested surfaces in principal stress space (Prevost, 1985). Their apex are fixed at the origin of axes but could be translated on the hydrostatic axis to take a small cohesion into account (for numerical purpose). The i-th surface is defined through

$$\mathrm{f}^{\mathrm{i}} \equiv \frac{3}{2} \cdot \left(\mathbf{s} - \mathrm{p}' \cdot \boldsymbol{\alpha}^{\mathrm{i}}\right) : \left(\mathbf{s} - \mathrm{p}' \cdot \boldsymbol{\alpha}^{\mathrm{i}}\right) - \left(\mathrm{M}^{\mathrm{i}}\right)^2 \cdot (\mathbf{p}')^2 = 0 \tag{7}$$

where $\boldsymbol{\alpha}^{\mathrm{i}}$ is a kinematic deviatoric stress tensor defining the coordinates of the yield surface centre in deviatoric space and M^i is a material parameter denoting the aperture of the cone.

1.4 *Plastic flow rule*

The plastic potential $\mathbf{P} = \mathbf{P'} + \mathrm{P''} \cdot \boldsymbol{\delta}$ is decomposed into its deviatoric part which is associative,

$$\mathbf{P'} = \mathbf{Q'} \tag{8}$$

and its dilationnal part which is non-associative

$$\mathrm{P''} = \frac{1}{3} \cdot \frac{\eta^2 - \bar{\eta}^2}{\eta^2 - \bar{\eta}^2} \qquad \text{and} \qquad \eta = \frac{\left({}^{3}/_{2} \cdot \mathbf{s}:\mathbf{s}\right)^{\frac{1}{2}}}{\mathrm{p'}} \tag{9}$$

where $\bar{\eta}$ is a material parameter that takes into account the phase transformation line (Ishihara, et al., 1975). This parameter rules the dilationnal behaviour and separates the p'-q plane into two zones. Stress ratios (η) lower than $\bar{\eta}$ imply a plastic contractive behaviour under shear loading while the other zone depicts a dilative plastic behaviour.

1.5 *Hardening rule*

The hardening rule is purely kinematic. During loading, active surface moves up to contact the next one. All surfaces inside the active one stay tangential at the current stress state. The relationship between plastic function and kinematic hardening is determined through the consistency condition (Prevost, 1985) and leads to

$$\mathrm{p'} \cdot \dot{\boldsymbol{\alpha}}^{\mathrm{i}} = \frac{\mathrm{H'}}{\mathbf{Q'}:\boldsymbol{\mu}} \cdot \langle \mathrm{L} \rangle \cdot \boldsymbol{\mu} \tag{10}$$

where $\boldsymbol{\mu}$ is a tensor defining the direction of translation of the active surface in the deviatoric space. At this step, any direction of translation could be used. The only requirement is that the outermost activated surface has to be at most tangential to the next one, at the end of a given step. The overlapping of surfaces is then avoided. In the original paper, the Mroz rule was chosen. This choice enforces an explicit integration of the law.

$$\boldsymbol{\mu} = \frac{\mathrm{M}^{\mathrm{i}+1}}{\mathrm{M}^{\mathrm{i}}} \cdot \left(\boldsymbol{s} - p' \cdot \boldsymbol{\alpha}^{i}\right) - \left(\boldsymbol{s} - p' \cdot \boldsymbol{\alpha}^{i+1}\right) \tag{11}$$

1.6 *Refinements*

Dependency on stiffness (bulk, shear and plastic moduli) for the mean effective stress is taken into account through (Prevost, 1985)

$$\mathrm{X}(\mathrm{p'}) = \mathrm{X}_0 \cdot \left(\frac{\mathrm{p'}}{\mathrm{p_r}}\right)^{\mathrm{n}} \qquad where\ X = \{K, G, H'\} \tag{12}$$

where p_r is a reference pressure and X_0 is the corresponding stiffness at p_r. Typically n equals 0.5 for sands (Prevost, 1985) . Other shapes of surfaces can be considered. The Lode-angle dependency is taken into account through the use of Van Eekelen surfaces (Yang, et al., 2008; Zerfa, et al., 2003).

2 COMPARISON WITH LABORATORY TESTS

2.1 *Calibration*

A series of tests on Nevada sand, available in the scope of VELACS project (Arulmoli, et al., 1992), was used as experimental background. It provides a large number of triaxial monotonic and cyclic tests at several densities.

Elastic parameters for modelling are available in (Popescu, et al., 1993). Monotonic triaxial tests in both compression and extension are used to calibrate the basic plastic parameters of the model (Zerfa, et al., 2003). For a triaxial test, Equation (7) describing the i-th surface depends only on 2 scalars parameters (α^i et m^i) and is transformed into

$$\mathrm{f} \equiv \left(\mathrm{q} - \alpha^{\mathrm{i}} \cdot \mathrm{p'}\right)^2 - \left(\mathrm{m}^{\mathrm{i}}\right)^2 \cdot (\mathrm{p'})^2 = 0 \tag{13}$$

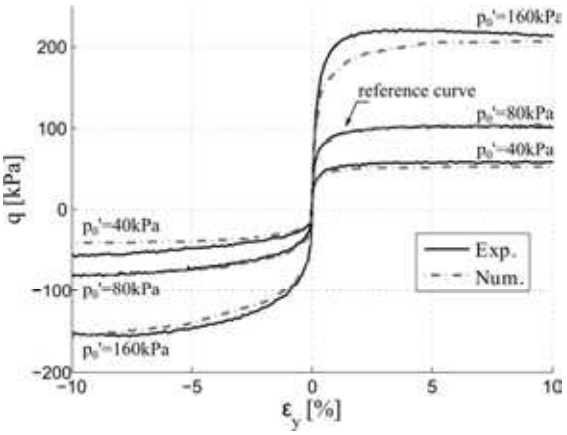

Fig. 1. Comparison between experimental p'-constant drained triaxial tests (Arulmoli, et al., 1992) and numerical modelling for Nevada Sand (Dr=40%) : deviatoric stress vs. vertical deformation. Tests are available for 3 different initial mean effective pressures (40-80-160 kPa) in compression and extension.

Parameters related to the surfaces are obtained from drained tests:

1. An experimental q-ϵ_y curve (deviatoric stress vs. vertical deformation) in compression is delimited into linear segments along which plastic moduli are constant. The number of segments corresponds to the number of surfaces. Transitions from a surface to another give initial upper bounds of surfaces.
2. The procedure is repeated for an experimental extension curve at the same initial mean effective pressure but plastic modulus are already known. The lower bound of each surface is then found. Aperture (M^i) and initial position (α^i) of the centre of each surface are then computed.

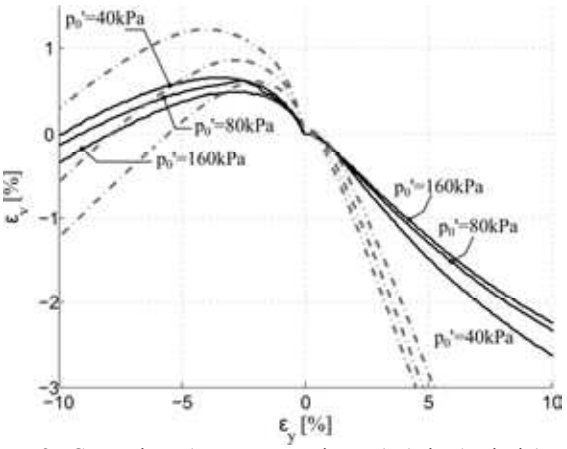

Figure 2. Comparison between experimental drained triaxial tests (Arulmoli, et al., 1992) and numerical modelling for Nevada Sand (Dr=40%) volumetric vs. vertical deformation. Tests are available for 3 different initial mean effective pressures (40-80-160 kPa).

The p'=80kPa curve was adopted as a reference curve for calibration. The model is then applied to other initial mean pressures. Results in the q-ϵ_y plane are given in Fig. 1. Numerical and experimental curves fit relatively well. However, regarding the volumetric deformation, the numerical curves don't match the tendency of experimental ones. The only parameter $\bar{\eta}$ that rules the plastic potential is the cause of those discrepancies. The phase transformation line is accurately defined in the p'-q plane but the amount of contractancy or dilatancy is not adjustable.

Fitting of the monotonic curves can be considerably improved considering a modified plastic potential (in Figure 3). The potential is split into a near field (small η) in which the potential is the original one and a far-field (large η) in which the potential is modified. Only two new parameters are necessary.

$$P'' = \frac{1}{3} \cdot \frac{\eta^2 - \bar{\eta}^2}{\eta^2 - \bar{\eta}^2} \cdot \left(1 + \frac{2}{\pi} \cdot \tan^{-1}\left(\frac{|\eta|}{\eta_2}\right) \cdot (\eta_3 - 1)\right) \quad (14)$$

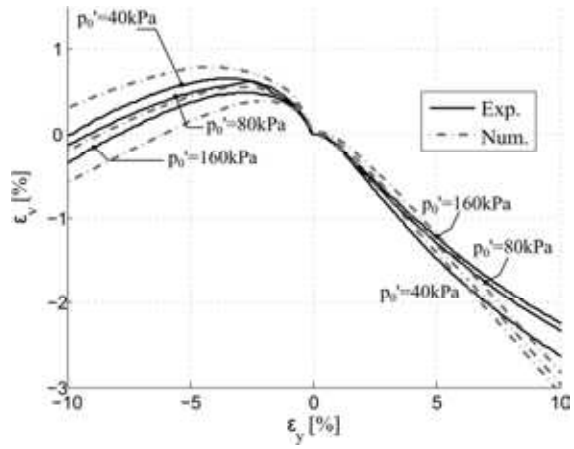

Figure 3. Comparison between experimental drained triaxial tests (Arulmoli, et al., 1992) and numerical modelling for Nevada Sand (Dr=40%) volumetric vs. vertical deformation. Tests are available for 3 different initial mean effective pressures (40-80-160 kPa).

Insufficiency of this adaptation is obvious in Figure 4. A cyclic behaviour is modelled, based on parameters obtained above. Stress path in p'-q plane is quite different but moreover, the q-ϵ_y curve doesn't match and isn't represented here. An accurate modelling of cycles in both q-p' and q-ϵ_y planes definitely requires a more complex expression of the plastic potential such as in (Elgamal, et al., 2003). The immediate consequence is an increase in the number of state parameters necessary to describe the model, though the number of laboratory tests increases.

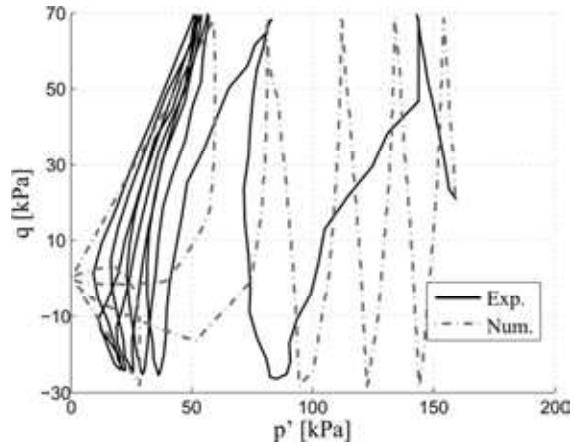

Figure 4. Comparison between experimental drained triaxial tests (Arulmoli, et al., 1992) and numerical modelling (with modified plastic potential) for Nevada Sand (Dr=40%) deviatoric vs. mean effective stress.

Despite its drawbacks, the Prevost's model can qualitatively capture the main features of the cyclic behaviour of a soil: pore pressure build up (Zerfa, et al., 2003) and plastic deformation accumulation. Hence it's better than classical isotropic hardening models to represent cyclic behaviour of soils.

3 PRACTICAL EXAMPLE: SUCTION CAISSON

The advantages of the model are shown through an application, based on (Vertseele, 2012). The case study is a suction caisson part of a tripod foundation for wind turbine firstly loaded by the dead weight and then submitted to a cyclic loading. The latter consists of two phases of loading with different amplitudes (period=10s). The second amplitude is twice the first one. Results obtained from the Prevost's model (PR) are compared to the classical Drucker-Prager model (DP). The PR model is used in its basic form since the proposed modification of the plastic potential doesn't improve the fitting of the cyclic behaviour. Furthermore, the p'-dependency of the stiffness is not taken into account ($n = 0$) because the DP model implemented in the code is not able to represent it.

3.1 *Geometry*

In order to simplify comparison, the mesh is supposed axisymmetric and the horizontal load is neglected. The loading is only a compression/decompression vertical force. The caisson has a diameter of 8m and a skirt depth of 4m. The total mesh size is 24mx22m to avoid problems with boundaries. There are 1892 finite coupled elements (from FE code LAGAMINE). Parameters are those obtained for a Nevada Sand isotropically consolidated at a relative density of 60% (Table 1).

Table 1. Parameters characterizing the models. Elastic parameters (E,ν) and permeability are common to both models. ϕ_0 and ϕ_f are respectively the initial and final friction angle of the DP model whilst ψ is the dilatancy angle.

Com.	Elastic	E (kPa)	2,7.105				ν (/)		0.25	
	k (m/s)	1.10^{-5}								
PR model	Surface	1	2	3	4	5	6	7	8	9
	H' (kPa)	5.10^4	4.10^4	3.10^4	2.10^4	1.10^4	7.10^3	2400	1000	300
	α^i (/)	0.065	0.135	0.220	0.250	0.325	0.400	0.400	0.400	0.385
	m^i (/)	0.165	0.265	0.380	0.450	0.575	0.700	0.900	1.050	1.165
	$\bar{\eta}$	0.7								
DP	ϕ_0(°)	10					ϕ_f (°)		42	
	ψ (°)	4.5								

3.2 *Results*

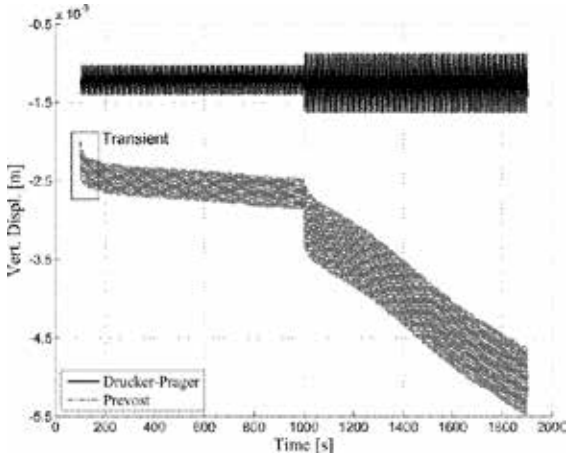

Figure 5. Comparison between vertical displacement at 0.5m depth under the top of the suction caisson for PR and DP models.

The first comparison in Figure 5 depicts the accumulation of vertical displacement of the soil under the top of the caisson. The weight of the wind turbine causes the first initial displacement. Afterwards, the behaviour under cyclic loading is quite different. For the DP model, the displacement oscillates between nearly fixed boundaries and the soil lies within the elastic zone most of the time. Actually the median displacement is not exactly constant but changes very slightly at the beginning of both loading phases.

On the other hand the PR's model clearly shows an accumulation of vertical displacement at each cycle. Moreover during the first phase, transient and stationary behaviours can be distinctly observed. The change in amplitude of loading implies a change in the tendency of accumulation.

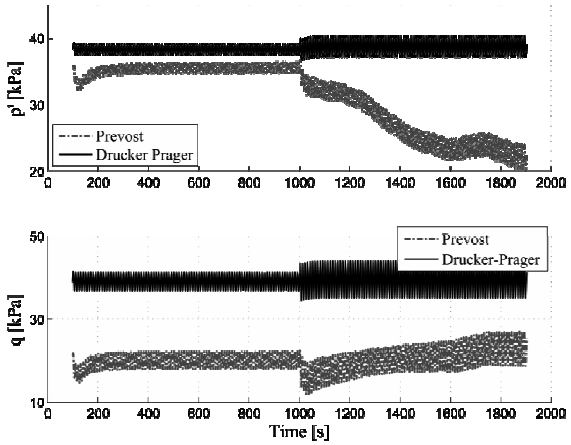

Figure 6. Comparison between mean effective and deviatoric stresses at 0.5m depth under the top of the suction caisson for PR and DP models.

Corresponding evolutions of mean effective and deviatoric stresses are shown in Figure 6 while pore pressure accumulation is given in Figure 8. During the first part of the loading, the difference between both models is limited. For the Prevost's model, the transient phase is short and a drop in mean effective stress is coupled with an increase of pore water pressure. Then a stationary phase takes place, corresponding to an accommodation phase (see in Figure 7) and the mean effective pressure gets back to its first value when pore water pressure dissipates. The difference is quantitatively greater for the deviatoric stress but qualitatively the behaviour is identical.

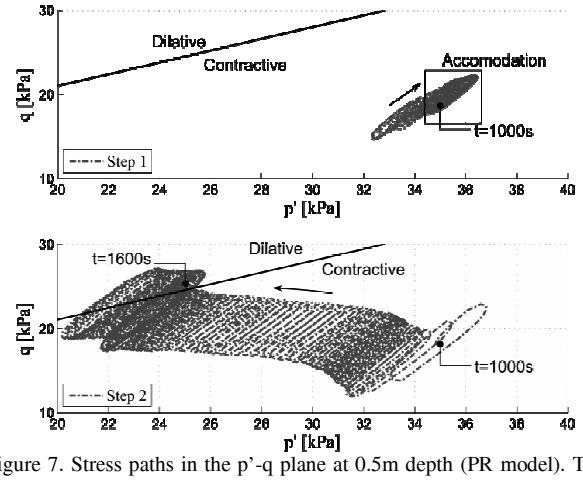

Figure 7. Stress paths in the p'-q plane at 0.5m depth (PR model). The first step of loading ends after 1000s when the second begins.

During the second part of loading, the soil characterized by PR model shows a continuous decrease of mean effective stress without reaching a stationary state. Greater amplitude of loading entails greater plasticity effects and then contractancy. After about 1600s, the stress path reaches the phase transformation line and the mean effective stress increases for a while before going down again. This continuous contractancy appears because the model involves plasticity in loading and unloading as well as a transition between contractive and dilative zones. On the other hand, the soil described by DP model behaves elastically most of the time because once the greatest deviatoric stress is reached, the stress path lies within the plasticity surface when unloaded and reloaded.

4 CONCLUSIONS

The Prevost's model is simple, elegant and able to qualitatively take into account the main features of cyclic loading. Basic parameters are easy to obtain from classical laboratory tests. Nevertheless an accurate modelling of cyclic tests requires additional parameters and a new form of plastic potential.

A suction caisson was modelled as a practical case study. Capabilities of the Prevost's model compared with a classical Drucker-Prager model appear clearly. The transient modelling depicts pore pressure and plastic deformation accumulation which the Drucker-Prager model is unable to represent.

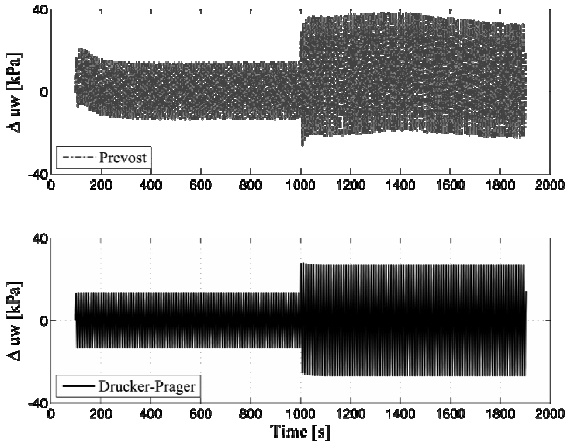

Figure 8. Comparison between pore pressure evolutions at 0.5m depth under the top of the suction caisson for PR and DP models.

5 ACKNOWLEDGEMENTS

I would warmly acknowledge all people that help me daily to achieve this PhD and my colleagues that suffer my little idiosyncrasies. I would also thank the FNRS for its financial support.

6 REFERENCES

Arulmoli, K., et al. 1992. *Verification of Liquefaction Analyses by Centrigue Studies, Laboratory Testing Program, Soil Data Report.* .

Elgamal, Ahmed, et al. 2003. Modeling of cyclic mobility in saturated cohesionless soils. *Internation Journal of Plasticity.* 2003, Vol. 19, pp. 883-905.

Houlsby, G. T., Ibsen, L. B. et Byrne, B. W. 2005. *Suction caissons for windturbines.* Perth , Australia : International Symposium on Frontiers in Offshore Geotechnics (ISFOG).

Ishihara, K., Tatsuoka, F. et Yasuda, S. 1975. Undrained deformation and liquefaction of sand under cyclic stresses. *Soils and foundations.* 1975, Vol. 15, 1, pp. 29-44.

Popescu, R. et Prevost, J.-H. 1993. Centrifuge validation of a numerical model for dynamic soil liquefaction. *Soil Dynamics and Earthquake Engineering.* 1993, Vol. 12, pp. 73-90.

Prevost, J.H. 1985. A simple plasticity theory for frictional cohesionless soils. *Soil Dynamics and Earthquake Engineering.* 1985, Vol. 4, 1, pp. 9-17.

Vertseele, H. 2012. *Cyclic loading of suction caisson foundations for offshore wind turbines.* University of Liège. 2012. Master Thesis.

Yang, Zhaohui et Elgamal, Ahmed. 2008. Multi-surface Cyclic Plasticity Sand Model with Lode Angle Effect. *Geotechnical and Geological Engineering.* June 2008, Vol. 26, 3, pp. 335-348.

Zerfa, F. Z. et Loret, B. 2003. Coupled dynamic elastic-plastic analysis of earth structures. *Soil dynamics and Earthquake Engineering.* 2003, Vol. 23, pp. 435-454.